

The Anisotropic Transfer of Resonance Photons in Hot Plasmas on Magnetized White Dwarfs

Yukikatsu TERADA¹, Manabu ISHIDA², Kazuo MAKISHIMA^{1,3}

¹*Cosmic Radiation Laboratory, RIKEN,*

2-1 Hirosawa, Wako, Saitama, 351-0198 Japan

terada@riken.go.jp

²*Department of Physics, Tokyo Metropolitan University,*

1-1 Minami-Ohsawa, Hachioji-shi, Tokyo, 192-0397 Japan

ishida@phys.metro-u.ac.jp

³*Department of Physics, Science, The University of Tokyo,*

7-3-1, Hongo, Bunkyo-ku, Tokyo, 113-0033 Japan

maxima@phys.s.u-tokyo.ac.jp

(Received 2003 July 22; accepted 0 0)

Abstract

In order to confirm the anisotropic effect of resonance photons in hot accretion columns on white dwarfs in magnetic cataclysmic variables, proposed by Terada et al.(2001), systematic studies with *ASCA* of 7 polars and 12 intermediate polars are performed. The equivalent widths of He-like Fe K_{α} line of polars are found to be systematically modulated at their spin periods in such a way that it increases at the pole-on phase. This implies that the anisotropic mechanism is commonly operating among polars. On the other hand, those of intermediate polars are statistically consistent with being unmodulated with an upper limit of 1.5 times modulation. This may be due to a different accretion manner like aurora curtain (Rosen et al. 1988) so that the plasma becomes optically thin along the horizontal axis also for the resonance lines, or because of larger optical depths for Compton scattering if the emission regions have the same coin-like shapes as polars.

Key words: X-rays:general — accretion — plasmas — scattering — white dwarfs

1. Introduction

A magnetic cataclysmic variable (MCV) is a close binary consisting of a white dwarf (WD) and a mass-donating companion star. Matter that spills over the Roche lobe of the companion star accretes on a magnetic pole of the WD, forming a post-shock hot plasma

(Patterson 1994 and references therein). According to the systematic X-ray study of MCVs by *Ginga*, their X-ray spectra can be described by optically thin thermal bremsstrahlung continua with Fe lines (Ishida 1991). These X-ray characteristics are approximately the same for both subgroups of MCVs, polars and intermediate polars (IPs). Plasma diagnostics with atomic lines, performed with *ASCA* (Fujimoto and Ishida 1997; Ezuka and Ishida 1999), confirmed the multi-temperature structure of the plasma as had been predicted by Hoshi (1973) and Aizu (1973).

Considering the typical size ($\sim 10^7$ cm) and density ($\sim 10^{15-16}$ cm $^{-3}$) of an accretion column of an MCV, the plasma is not completely optically thin; it is estimated to be marginally optically thick for Compton (or Thomson) scattering with an optical depth of order 0.1. Under such conditions, the atomic line structure is expected to be suppressed by 10%–20%, because the line photons would experience large shifts reaching ~ 1 keV as they Compton scatter off hot electrons. At the same time, the plasma is optically thick for resonant photons of atomic lines from abundant heavy elements, including Fe in particular (Fujimoto and Ishida 1997). Then, the line structure of resonance transitions would be more suppressed, because the resonant photons would be effectively trapped in the column, and escape most easily when they Compton scatter out of the resonance. Nevertheless, we usually observe many ionized atomic lines in the X-ray spectra of MCVs (Ezuka and Ishida 1999), and apparent metal abundances derived from the equivalent width (EW) of these lines are not much lower than one times solar. In addition, some MCVs called Pole-on line emitters (POLES; Paper I), including AX J2315–0592 (Misaki et al. 1996), RX J1802.1+1804 (Ishida et al. 1998), and AX J1842.8–0423 (Terada et al. 1999), exhibit extremely strong He-like Fe-K lines, having an EW of ~ 4000 eV, implying apparent Fe abundances of \sim three times solar.

In order to solve the puzzle of extremely strong Fe lines, we have developed a scenario of Fe-K line collimation along the vertical axis of the accretion column incorporating resonance scattering (Terada et al. 1999; Terada et al. 2001, hereafter Paper I; Terada 2002). The anisotropy occurs when the accretion column has a flat shape, and is augmented by the strong longitudinal velocity gradient in the accretion flow, which invalidates the resonance condition for line photons when they propagate along the vertical axis. Since the Fe ions are heavy, their thermal resonance width (typically ~ 3 eV for a 10 keV plasma) is easily exceeded by the vertical Doppler shift (~ 10 eV from the bottom to the top of the column). Therefore, the resonant trapping of Fe-K photons is preferentially reduced along the vertical axis, and hence the resonance line photons are collimated along the vertical direction. This scenario can explain both the lack of line destruction and the enigmatic POLE phenomenon.

We have numerically confirmed the anisotropic propagation of resonance photons via extensive Monte Carlo simulations (Paper I), employing the analytic solution to the post-shock flow by Aizu (1973). The results show that the directional emissivity of the resonant Fe-K line photons is indeed enhanced up to a factor of ~ 2 –2.5. In addition, we have confirmed,

through *ASCA* observations of the polar V834 Centauri, that the EW of its He-like Fe K_α line increases during pole-on phases of its rotation (Paper I). The proposed mechanism has thus been confirmed through calculation, and observation of a few particular polars.

According to our Monte Carlo simulations, the anisotropic propagation of resonance Fe-line photons should occur for a rather wide range of plasma parameters in the accretion column (Paper I). We hence expect to observe the rotational modulation of the resonant Fe-K line EW, not only in the particular case of V834 Centauri, but also of MCVs in general. In order to examine this conjecture, here we systematically analyze the *ASCA* data of 7 polars and 12 IPs.

2. Observation

The central aim of this paper is to search the data for the possible dependence of the Fe line EW on the angle, θ , between our line-of-sight and the axis of the accretion column. We therefore need to perform spin-phase-resolved spectroscopy of the target MCVs. Accordingly, we have analyzed all the 9 polars and 13 IPs observed with *ASCA* satellite (Tanaka et al. 1994). After discarding objects which are too X-ray faint (< 0.05 GIS cnt s^{-1}) and those with insufficient exposure (< 20 ksec), we are left with 7 polars and 12 IPs, as listed in table 1, including V834 Centauri, results for which are reported in Paper I. Some objects (V834 Cen, EK UMa, and RX J1015+0904) are the approved targets of our proposal for this purpose, and the others are archived or published observations. Their geometries, i.e., the inclination angle i and the pole colatitude β , are obtained by polarimetric observations in the optical to ultraviolet band, and summarized in table 4 of Paper I.

For each target, we accumulated the GIS (Ohashi et al. 1996; Makishima et al. 1996) and SIS (Burke et al. 1991) events within a circle of radius $4'.5$ centered on the object, employing the following data-selection criteria. We discarded the data during *ASCA* passage through the South Atlantic Anomaly, and when the field of view of *ASCA* was within 5° of the Earth's rim. Furthermore, we discarded the GIS data during occasional errors in the on-board CPU, as well as the SIS data acquired when the field of view was within 10° of the bright Earth rim or when the spacecraft crossed the day-night transition zones.

3. Data Analysis and results

3.1. X-ray light curves

To perform the phase resolved analysis, we folded X-ray light curves of the selected objects in table 1 on their rotational periods. As shown in figure 1, the polars mostly exhibit single-peaked folded light curves in the high-energy band, indicating that we are observing a single pole. The deep X-ray minima seen in some polars to higher energies are due to the self-eclipse of the emission region, while the residual mild X-ray intensity modulations during the

uneclipsed phase are explained in terms of the varying contribution from the scattered and/or reflected component from the surface of the white dwarfs (Beardmore et al. 1995). Therefore, the phase of the maximum X-ray intensities roughly corresponds to the pole-on phase ($\theta \sim 0$), or the phase where our line of sights comes closest to the accretion-column axis (minimum θ). In addition, in figure 1, the light curves often exhibit absorption dips in softer energies at the X-ray maximum phase. Since these dips arise due to photoelectric absorption by pre-shock matter in the accretion column, they can be used as an additional indicator of the pole-on phase. In this way, we have determined the pole-on and side-on phases of our target sources, as shown by the gray and black bands, respectively, in figure 1. Utilizing the geometric parameters summarized in table 4 of Paper I, we have excluded the phase of $\theta > 90^\circ$, in which the emission region is eclipsed by the white dwarfs.

For the phase determination of the IPs shown in figure 2, we have to rely solely on the X-ray spin modulations, because of the lack of optical polarization. According to the phase-resolved spectroscopy with *Ginga* (Ishida 1991), the X-ray minimum phase is thought to correspond to the pole-on phase, because the X-ray modulation is due to photoelectric absorption by the pre-shock matter (Rosen et al. 1988), as evidenced by the deeper X-ray modulations in softer energy bands. This idea of self-absorption is supported by Doppler measurements of He II emission lines from the pre-shock matter (Hellier et al. 1987, 1990). We have thus defined the pole-on and side-on phases as shown by the gray and black bands, respectively, in figure 2.

3.2. Phase-resolved spectra

We have accumulated the *ASCA* spectra separately over the pole-on and side-on phases, as shown in figures 3 and 4 for the polars and intermediate polars, respectively. To quantify the EWs of the Fe lines, we adopted the standard spectral model, i.e., a photoelectrically absorbed bremsstrahlung continuum with three narrow Gaussians (Ezuka and Ishida 1999; Paper I), the latter representing neutral (at 6.4 keV), He-like (at ~ 6.7 keV), and H-like (at ~ 6.9 keV) Fe- K_α lines. The three lines can be resolved with the SIS, but not with the GIS. Accordingly, we fixed the centroid energies of the first Gaussian at 6.4 keV, fixed the ratio of the centroid energies of the others at the theoretical value of 1.042, and assumed them to be narrow. The energy range for the continuum fitting was optimized in the manner described in section 3.2 of Ezuka and Ishida (1999). The SIS and GIS spectra were fitted simultaneously. The fits are successful, as shown in figures 3 and 4, where we compare predictions of the best-fit model with the actual data.

Figure 5 compares the EWs of the H-like and He-like Fe- K_α lines of individual polars for their pole-on and side-on phases. Figure 6 presents the same comparison for the IPs. For reference, the EWs of the fluorescent Fe- K_α line, which is not emitted from the hot accretion columns but probably from the WD surfaces, are also plotted in the same figures. As is clearly

demonstrated by figure 5, the EWs of the He-like Fe line of our sample polars are systematically larger in the pole-on phase than in the side-on phase, although the enhancement in individual objects is insignificant, and that of the H-like line is consistent with being unmodulated. Quantitatively, the enhancement of the H-like and He-like Fe K lines, weighted by the absolute values of their EWs, are $\zeta_{\text{OBS}}^{\text{P}}(\text{H}) = 1.05 \pm 0.47$ and $\zeta_{\text{OBS}}^{\text{P}}(\text{He}) = 1.88 \pm 0.72$, respectively (90% confidence errors). The significance is slightly reduced to $\zeta_{\text{OBS}}^{\text{P}}(\text{H}) = 1.05 \pm 0.53$ and $\zeta_{\text{OBS}}^{\text{P}}(\text{He}) = 1.89 \pm 0.86$, when we exclude the data of V834 Centauri, which were already presented in Paper I. Our result for the sample of polars therefore confirms the enhancement of the He-like line in a statistical sense. For the IPs, we see no modulation in either Fe line (figure 6); the enhancement of the H-like and He-like Fe K lines are $\zeta_{\text{OBS}}^{\text{IP}}(\text{H}) = 1.02 \pm 0.47$ and $\zeta_{\text{OBS}}^{\text{IP}}(\text{He}) = 1.14 \pm 0.36$, respectively.

4. Discussion

In order to confirm the general validity of the anisotropic transfer scenario of resonance photons in MCVs pointed out in Paper I, we have systematically analyzed the *ASCA* data of 7 polars and 12 intermediate polars. Through phase-resolved analysis of the ionized Fe K_{α} lines, the EWs of the He-like Fe lines of the polars have been found to be systematically enhanced in their pole-on phases. Although the significance is only 90%, and the individual cases were insignificant except for V834 Centauri (Paper-I), the statistical trend is in support of our scenario. To better visualize this result, we plotted in figure 7 left panel the EWs of the He-like Fe lines of the polars relative to the phase averaged value, as a function of θ . There, we also plot the results of our Monte Carlo simulations based on representative parameters (see caption). Thus, the observed spin-phase dependence of the Fe-K line EWs is consistent with the calculation, although within rather large errors.

The observed He-like Fe line is in fact a blend of resonance, forbidden, and intercombination lines, where the latter two do not suffer the resonance effect. Since the H-like line is a pure resonance line, we may expect to observe a larger spin modulation for this line compared to that of the He-like blend. According to our Monte Carlo simulations (Paper I; Terada 2002), however, the expected enhancement of the H-like Fe line is actually smaller than that of the He-like resonance line, because the former photons are preferentially produced in a higher portion of the post-shock column, which has lower densities and smaller velocity differences than those at the bottom of the column (Aizu 1973). As presented in figure 8, we expect almost the same enhancement of H-like Fe line as that of the He-like blend. Furthermore, the H-like Fe-K line is subject to rather large measurement errors, due to its relatively poor statistics and its possible confusion with the Fe K_{β} emission line from He-like iron. As a result, the measurements of the H-like Fe line EWs (figures 5, 6, and 7 right) are consistent with the prediction.

As for IPs (figure 6), the modulations of both line species have been found to be statistically insignificant. One possible explanation is that the accretion streams of IPs have a

curtain-like shape (Rosen et al. 1988), with a much-reduced optical depth in the lateral direction, so that the anisotropic resonance effect is suppressed. Alternatively, the emission region may have a column shape like polars, and the lack of spin modulation in the Fe line EWs may be attributed to higher electron densities n_e in the plasma, as is indicated by their larger volume emission measure (VEM, described as $\int n_e^2 dV$, where V is the plasma volume) than those of polars. Then, the enhanced Compton scattering by hot electrons reduces the anisotropic effect on the resonance photons (see figure 8 in Paper I). In fact, by comparing figure 5 with figure 6, we find that the IPs exhibit systematically smaller EWs of Fe K lines than the polars.

In order to examine the latter possibility for the IPs, we plot in figure 9 VEMs of the polars and IPs listed in table 1, which shows that the VEMs of IPs are one-to-two orders of magnitude larger than those of polars. Then, adopting the same discussion as in section 5.2 of Paper I, we estimate that the accretion column of an IP has an order-of-magnitude higher electron density of $n_e \sim 10^{17} \text{ cm}^{-3}$, an order-of-magnitude lower column height of $h \sim 10^6 \text{ cm}$, and several times larger column radius of $r \sim 10^7 \text{ cm}$, all compared with polars. Under such conditions, the optical depth to Compton scattering is ~ 1.0 , whereas it is only 0.4 for polars. Therefore, the interpretation may actually work.

The Fe-K line photons provide the best diagnostics of the resonance effects, because Fe ions are massive enough for the thermal Doppler effect to fall significantly below the bulk-motion Doppler shift. Although the *ASCA* data of MCVs are rather limited both in statistics for phase-resolved analyses and energy resolution, a quantum jump in this research subject may be realized by the *ASTRO-E 2* satellite to be launched in 2005, with its energy resolution reaching $\sim 10 \text{ eV}$ around the Fe- K_α -line range for the first time.

Finally, we thank the members of the *ASCA* team for spacecraft operation and data acquisition.

References

- Aizu, K. 1973, *Prog. Theor. Phys.*, 49, 1184
 Augusteijn T., Heemskerk M. H. M., Zwarthoed G. A. A., van Paradijs J. 1994, *A&AS*, 107, 219
 van Amerongen S., Augusteijn T., and van Paradijs 1987, *MNRAS*, 228, 377
 Barwig H., Ritter H., Barnbantner O. 1994, *A&A*, 288, 204
 Beardmore A. P., Done C., Osborne J. P., and Ishida M. 1995, *MNRAS*, 272, 749
 Bond I. A., Bond I. A., Freeth R. V. 1988, *MNRAS*, 232, 753
 Buckley D.A.H., Haberl F., Motch C., Pollard K., Schwarzenberg-Czerny A., Sekiguchi K. 1997, *MNRAS*, 287, 117
 Burke B.E., Mountain R.W., Harrison D. C., Bautz M. W., Doty J. P., Ricker G. R., and Daniels, P.J. 1991, *IEEE Trans. Nucl. Sci.*, ED-38, 1069
 Cropper M., 1985 *MNRAS*, 212, 709
 Ezuka H. and Ishida M. 1999, *ApJS*, 120, 277

Fujimoto R. and Ishida M. 1997, ApJ, 474, 774
 Heise J. and Verbunt F. 1988, A&A, 189, 122
 Hellier C., Mason K. O., Rosen S. R., Cordova F. A. 1987 MNRAS, 228, 463
 Hellier C., Mason K. O. and Cropper M. 1990, MNRAS, 242, 250
 Hellier C. 1997, MNRAS, 288, 817
 Hoshi R. 1973, Progress of Theoretical Physics, 49, 776
 Ishida, M., Greiner, J., Remillard, R. A., Motch, C., 1998, A&A, 336, 200
 Ishida M. 1991, Ph.D thesis, University of Tokyo
 Kaluzny J. and Semeniuk I. 1988, IBVS 3145
 Makishima K., Tashiro M., Ebisawa K., Ezawa H., Fukazawa Y., Gunji S., Hirayama M., Idesawa E., Ikebe Y., Ishida M., Ishisaki Y., Iyomoto N., Kamae T., Kaneda H., Kikuchi K., Kohmura Y., Kubo H., Matsushita K., Matsuzaki K., Mihara T., Nakagawa K., Ohashi T., Saito Y., Sekimoto Y., Takahashi T., Tamura T., Tsuru T., Ueda Y., Yamasaki N. Y. 1996, PASJ, 48, 171
 Mennickent R. E., Diaz M. P., Arenas, J. 1999, A&A, 352, 167
 Mewe, R., Gronenschild, E. H. B. M., van den Oord, G. H. J. 1985, A&AS, 62, 197
 Misaki, K., Terashima, Y., Kamata, Y., Ishida, M., Kunieda, H., Tawara, Y. 1996, ApJ, 470, 53
 Norton A. J., Hellier C., Beardmore A. P., Wheatley P. J., Osborne J. P., Taylor P. 1997, MNRAS, 289, 362
 Ohashi T., Ebisawa K., Fukazawa Y., Hiyoshi K., Horii M., Ikebe Y., Ikeda H., Inoue H., Ishida M., Ishisaki Y., Ishizuka T., Kamijo S., Kaneda H., Kohmura Y., Makishima K., Mihara T., Tashiro M., Murakami T., Shoumura R., Tanaka Y., Ueda Y., Taguchi K., Tsuru T., Takeshima T. 1996, PASJ, 48, 1570
 Patterson J. P. 1994, PASP, 106, 209
 Piirola V., Coyne G. V., Takalo S. J., Takalo L., Larsson S., Vilhu, O. 1994, A&A, 283, 163
 Rosen S. R., Mason K. O., and Cordova F. A. 1988, MNRAS, 231, 549
 Schwöpe A. D., Cataln M. S., Beuermann K., Metzner A., Smith R. C., Steeghs D. 2000, MNRAS, 313, 533
 Schwöpe, A. D., Thomas, H. -, Beuermann, K., Reinsch, K. 1993, A&A, 267, 103
 Shafter A. W. and Macry J. D. 1987, MNRAS, 228, 193
 Skillman D. 1996, PASP, 108, 130
 Takano S., Koyama K., Tawara Y., Matsumoto T., Noguchi K., Iwata T., Takahashi N., Umemoto T., Tatematsu K., Ohashi N., Fukui Y. Makishima K. 1989, IAUC. 4745, 1
 Tanaka Y., Inoue H., Holt S. S. 1994, PASJ, 46, L37
 Terada Y., 2002, Ph.D thesis, University of Tokyo Japan
 Terada Y., Ishida M., Makishima K., Imanari T., Fujimoto R., Matstuzaki K., Kaneda H. 2001, MNRAS, 328, 112
 Terada Y., Kaneda H., Makishima K., Ishida M., Matsuzaki K., Nagase F. Kotani T. 1999, PASJ, 51, 39

Table 1. Objects analyzed in the present paper.

object name	Date of observation (UT)	Exp. (ksec)*		Cnt Rate		phase 0.0 (HJD) in figures 1 and 2	Spin period (days)	ref. [†]	
		SIS	GIS	SIS	GIS				
Polars									
V834 Cen	(1)	1994/03/03.64–04.13	21.7	23.2	0.26	0.18	2445048.9500	0.070498	1
	(2)	1999/02/09.93–11.72	62.3	53.5	0.25	0.19			
AM Her	(1)	1993/09/27.22–28.27	30.9	43.5	0.61	0.43	2443014.76614	0.128927	2
	(2)	1995/03/06.84–07.22	18.3	16.8	0.92	0.66			
	(3)	1995/03/09.03–10.03	45.5	41.1	0.89	0.65			
BL Hyi		1994/10/11.47–12.59	41.4	43.5	0.21	0.16	2450379.4725	0.078915	3
BY Cam		1994/03/11.49–12.16	29.5	34.7	0.98	0.68	2446138.8202	0.13979	4
EF Eri		1993/07/23.90–24.77	35.9	39.0	0.93	0.61	2443894.6824	0.056266	5
RXJ1015+0904		1999/05/04.08–05.41	54.0	54.0	0.09	0.07	2451302.500	0.055471	6
V2301 Oph		1998/09/28.49–30.21	70.6	73.0	0.21	0.15	2448071.02014	0.078450	7
Intermediate Polars									
AO Psc		1994/06/22.29–24.56	81.0	84.3	0.57	0.48	2444883.92074	0.00931948	8
BG CMi	(1)	1996/04/14.76–15.97	42.0	43.4	0.16	0.17	2450186.5	0.0105729	9
	(2)	1996/04/17.44–18.53	40.9	41.5	0.15	0.16			
EX Hya		1993/07/16.45–17.64	36.0	38.8	2.79	1.50	2437699.8914	0.0465465	10
FO Aqr		1993/05/20.93–02.04	37.8	38.0	0.27	0.32	2446097.243668	0.01451911	11
PQ Gem	(1)	1994/11/04.91–07.10	76.2	80.2	0.37	0.30	2449297.9730	0.009645994	12
	(2)	1999/10/19.71–20.31	35.0	42.9	0.37	0.28			
RXJ1712-2414		1996/03/18.85–21.24	81.4	84.2	0.79	0.65	2450159.5	0.010737	13
TV Col		1995/02/28.25–01.44	36.7	39.9	0.65	0.54	2447139.524	0.02211	14
TX Col		1994/10/03.29–04.42	39.9	45.1	0.22	0.16	2449627.5	0.02212	6
V1062 Tau		1998/02/16.89–18.48	57.5	14.7	0.23	0.24	2450859.5	0.04313	9
V1223 Sgr		1994/04/24.18–25.96	57.0	59.2	1.23	1.00	2445626.13067	0.00862854	17
V405 Aur	(1)	1996/10/05.56–07.47	47.5	41.1	0.34	0.23	2449689.573466	0.006313154	15
	(2)	1999/03/21.40–22.44	39.0	43.3	0.38	0.26			
XY Ari	(1)	1995/08/07.00–07.91	34.6	34.9	0.14	0.15	2449935.5	0.00238773	16
	(2)	1996/01/28.21–29.73	58.5	61.0	0.16	0.16			
	(3)	1996/02/18.97–19.56	24.4	25.6	0.13	0.14			

References; 1 Schwope et al. (1993), 2 Heise et al. (1988), 3 Mernickent et al. (1999), 4 Piirola et al. (1994), 5 Cropper (1985), 6 Norton et al. (1997), 7 Barwig et al. (1994), 8 Kaluzny et al. (1988), 9 Patterson (1994), 10 Bond et al. (1988), 11 Shafter et al. (1987), 12 Hellier (1997), 13 Buckley et al. (1997), 14 Augustejn et al. (1994), 15 Skillman et al. (1996), 16 Takano et al. (1989), and 17 *ASCA* Timing Analysis.

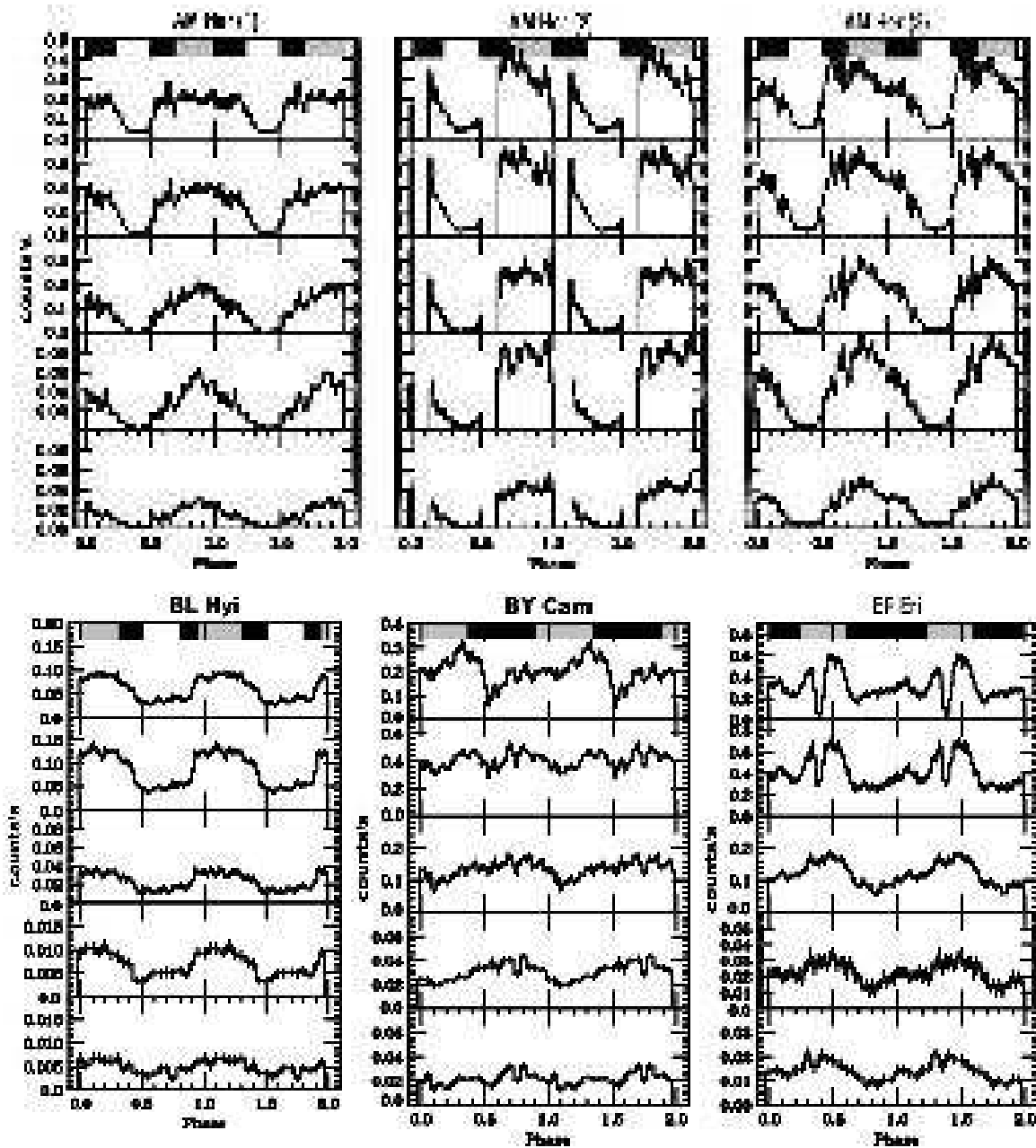


Fig. 1. X-ray light curves of the polars observed with *ASCA*, folded on their spin periods listed in table 1. The respective phase 0.0 is given in table 1. For each object, light curves in five energy bands (0.5–1.5, 1.5–4.0, 4.0–6.2, 6.2–7.2, 7.2–10.0 keV from top to bottom) are presented. The pole-on and side-on phases are shown at the top of each panel by the gray and black bands, respectively (see the text). The data of V834 Cen is reported in Paper I.

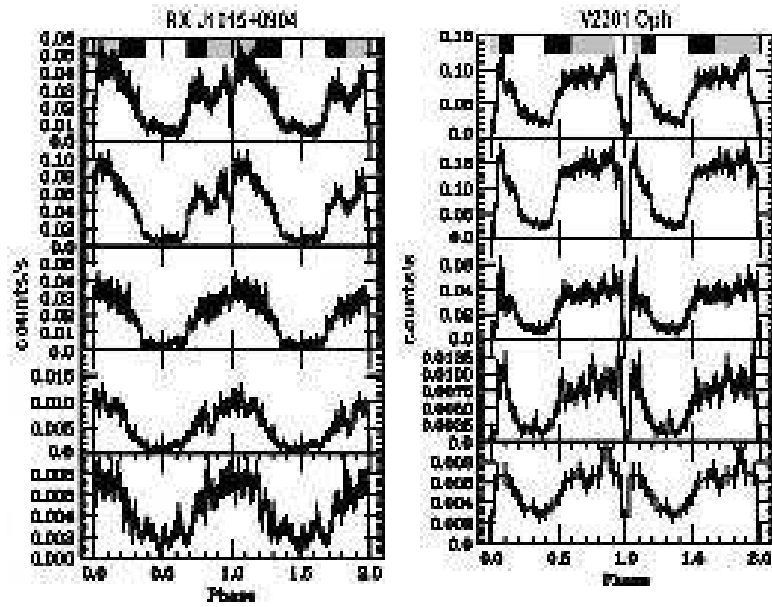


Fig. 1 Continued.

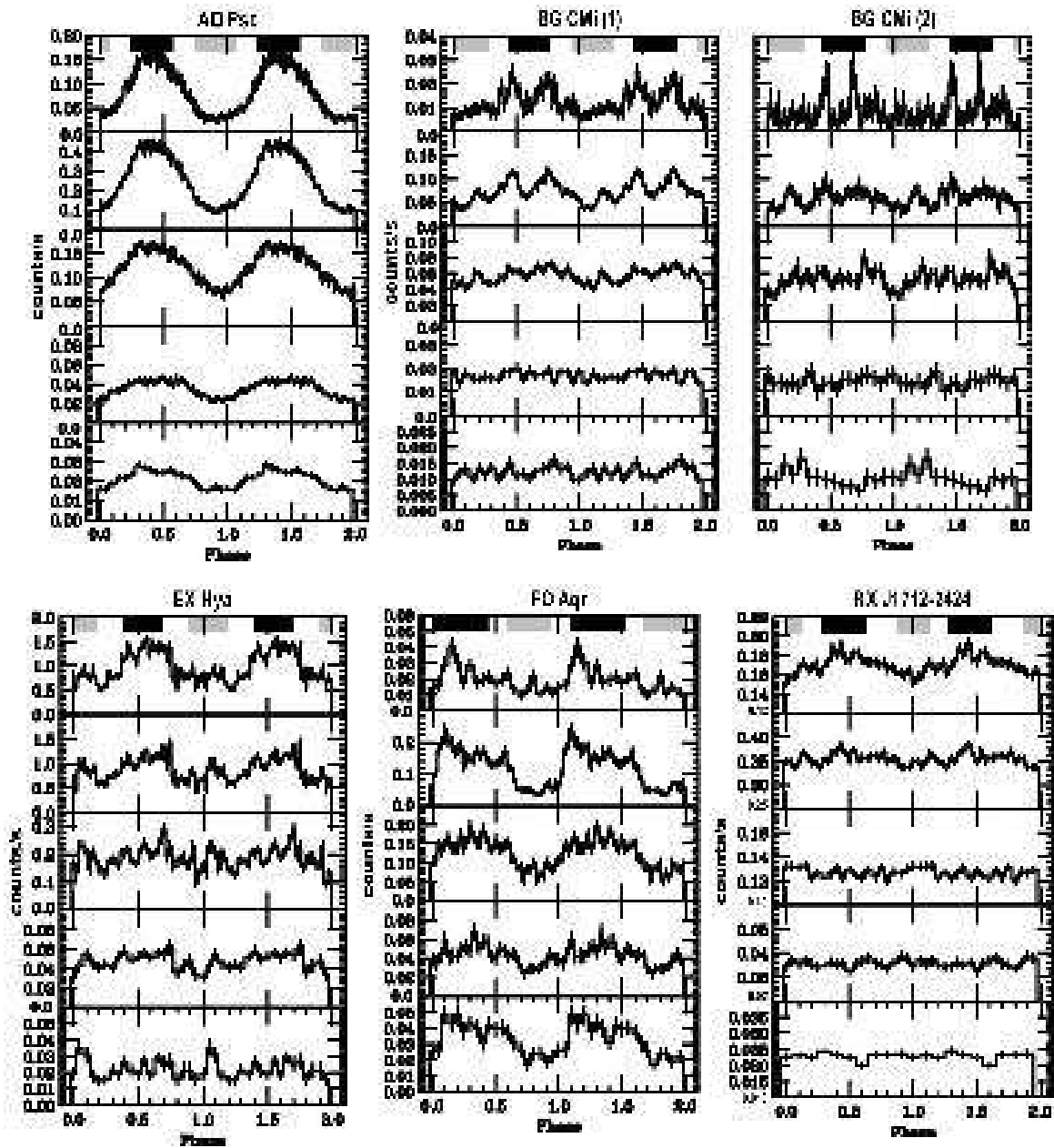


Fig. 2. Similar to figure 1, but for the IPs.

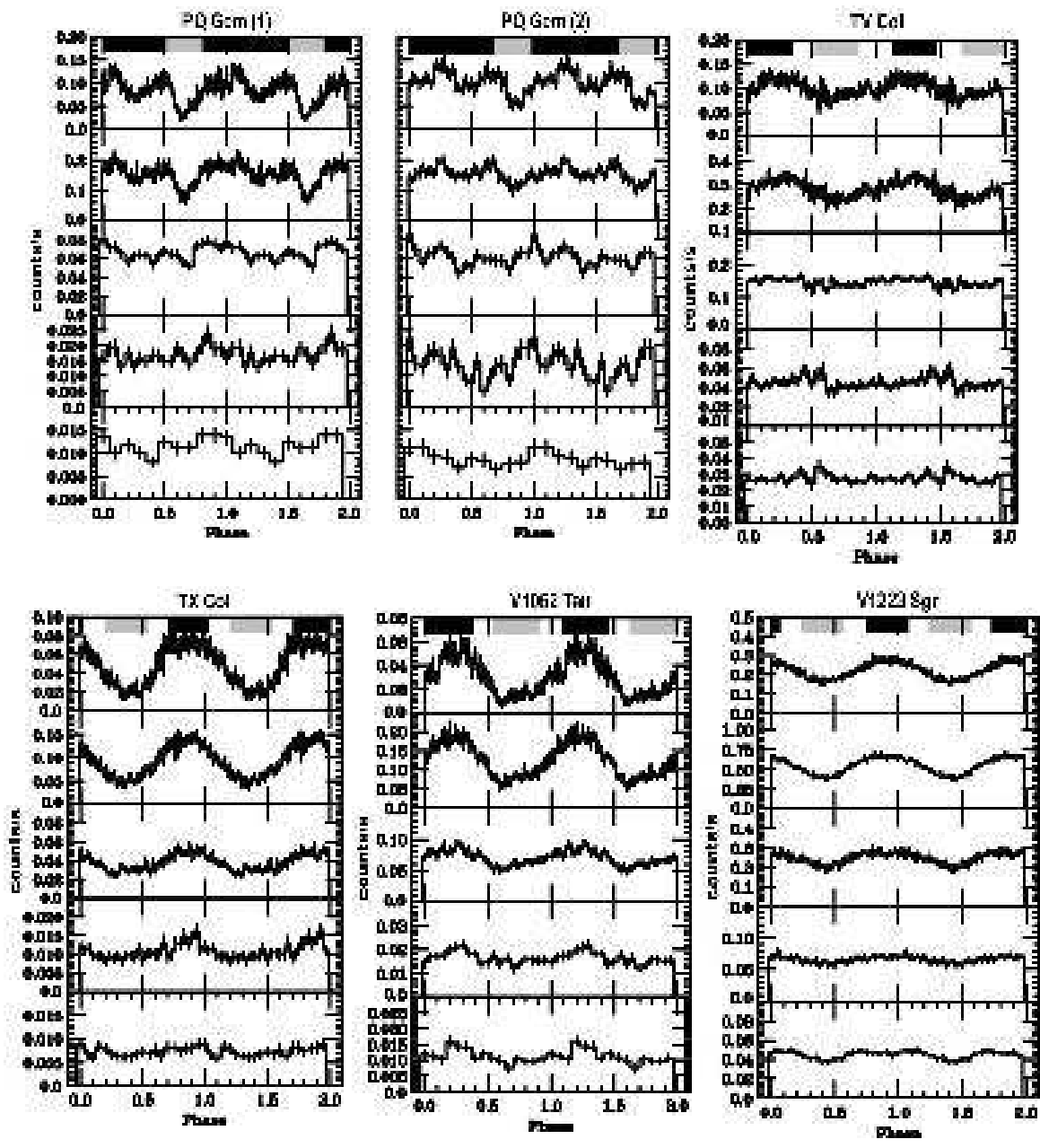


Fig. 2 Continued.

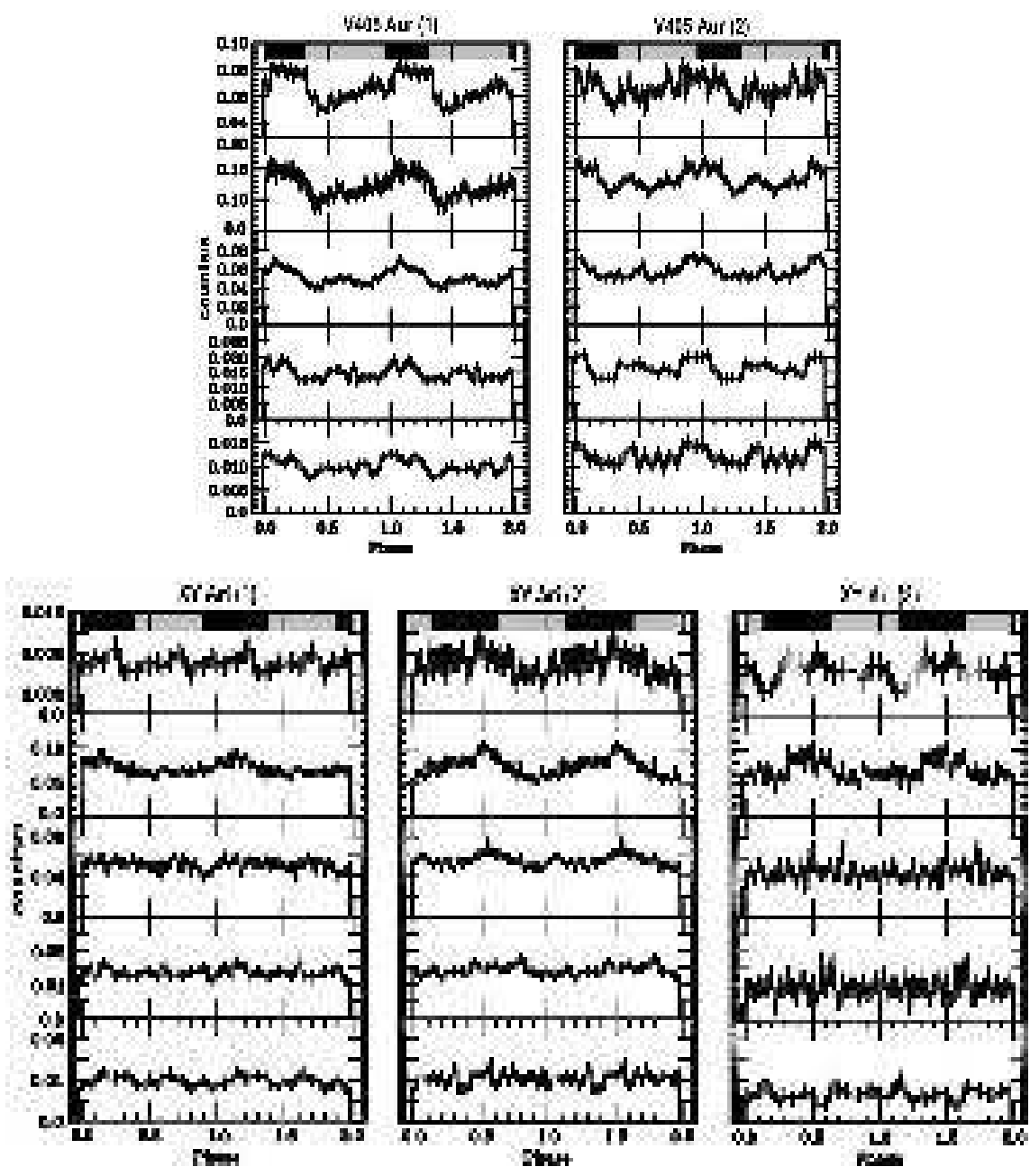


Fig. 2 Continued.

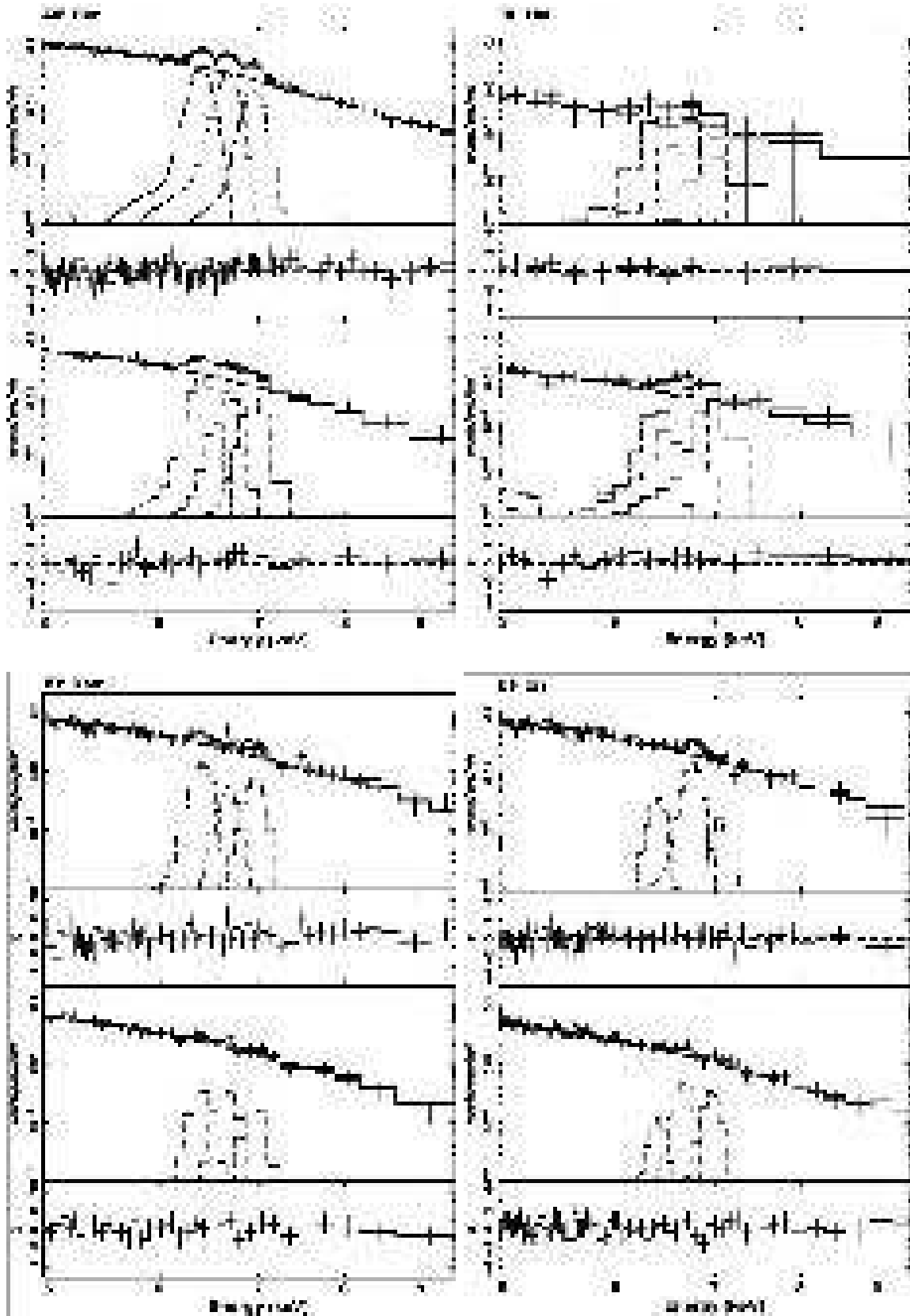


Fig. 3. Phase resolved spectra near the Fe energy band of the polars in our sample, acquired with *ASCA*. Top panels show the pole-on spectra, and bottom panels the side-on spectra. Only the SIS data are shown in this figure. The best fit models, obtained by simultaneous fitting the GIS and SIS data, are also plotted, after convolving with the detector response.

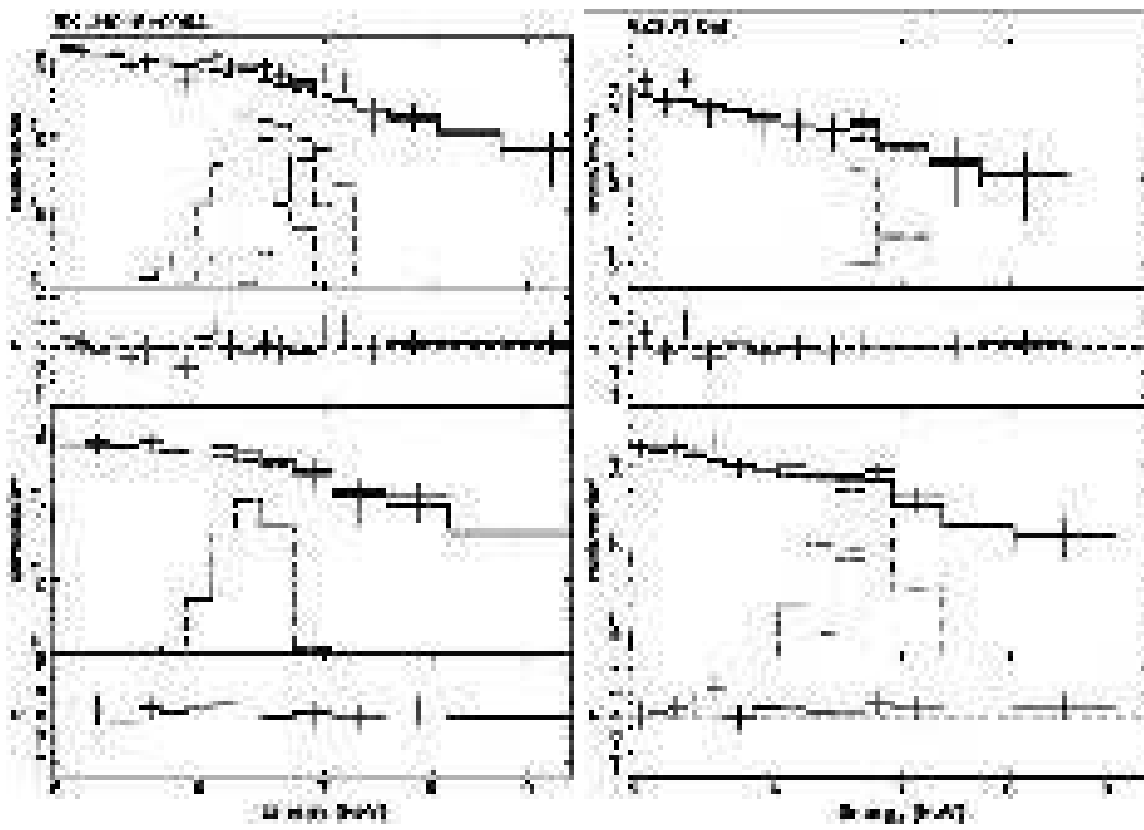


Fig. 3 Continued.

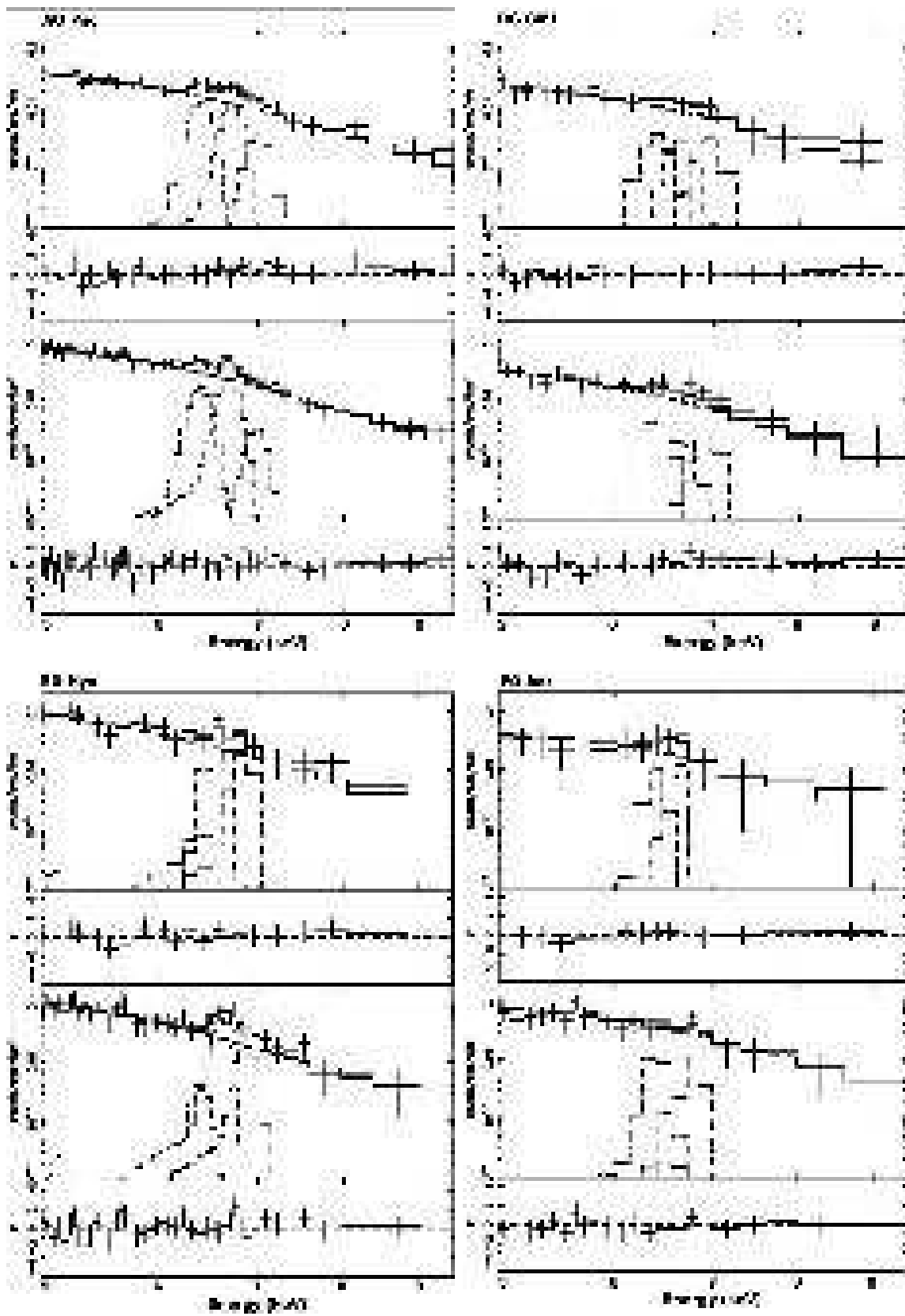


Fig. 4. Similar to figure 3, but for the IPs in our sample.

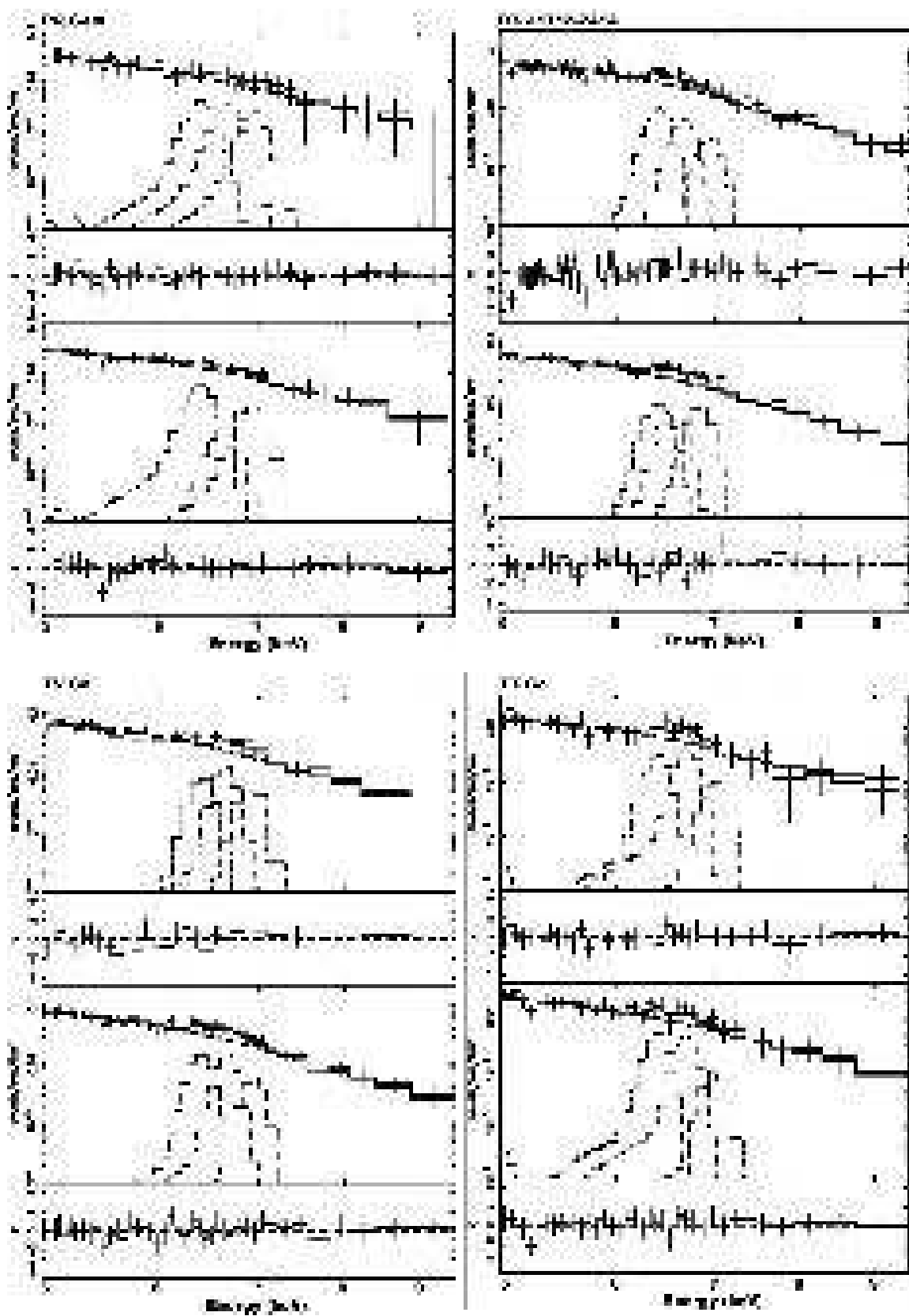


Figure 4 Continued.

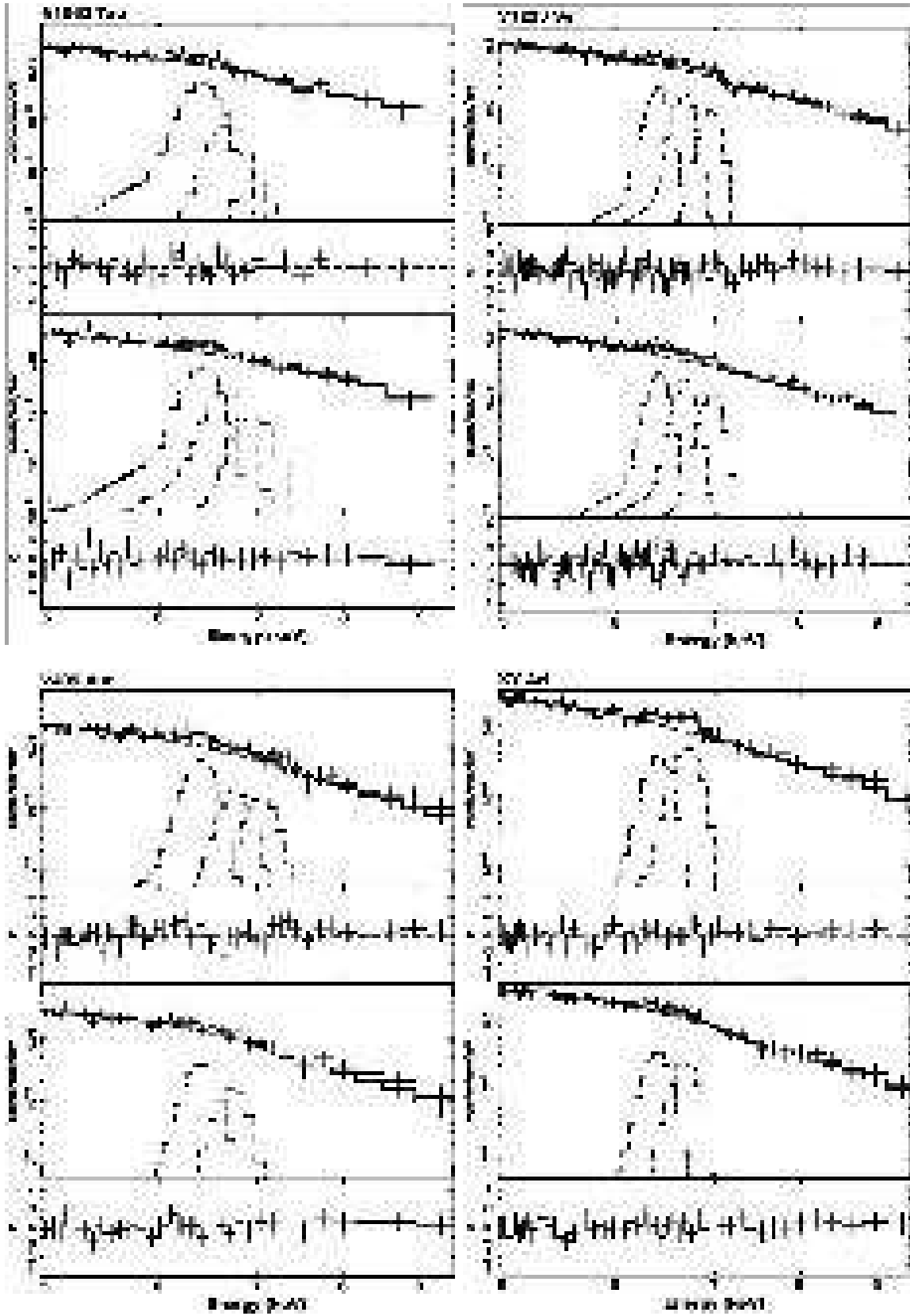


Figure 4 Continued.

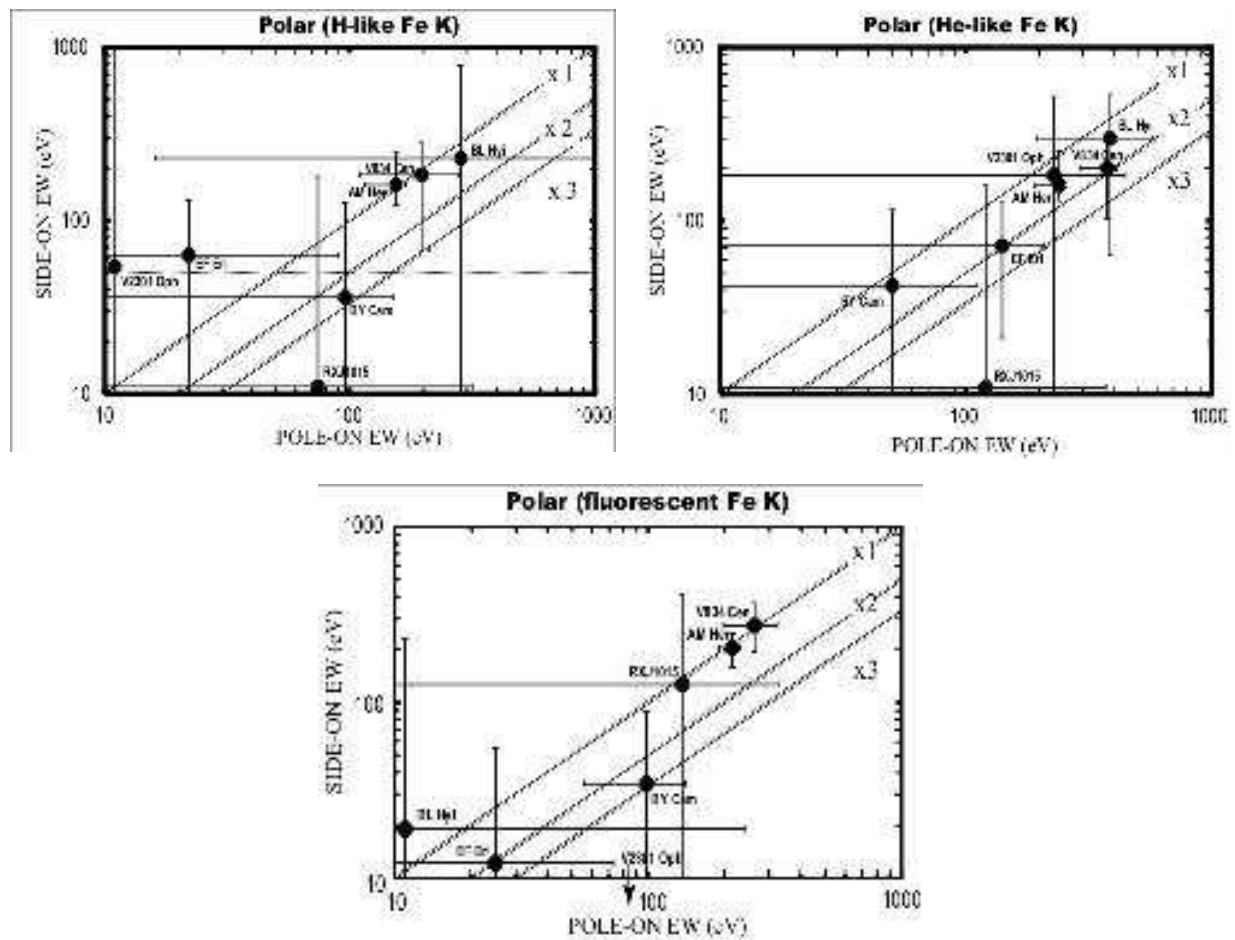


Fig. 5. The Fe line EWs of the polars measured at the pole-on phase, compared with those at the side-on phase. The top left and top right panels are for H-like and He-like Fe K lines, respectively. For reference, EWs of fluorescent Fe K lines are plotted in the bottom panel.

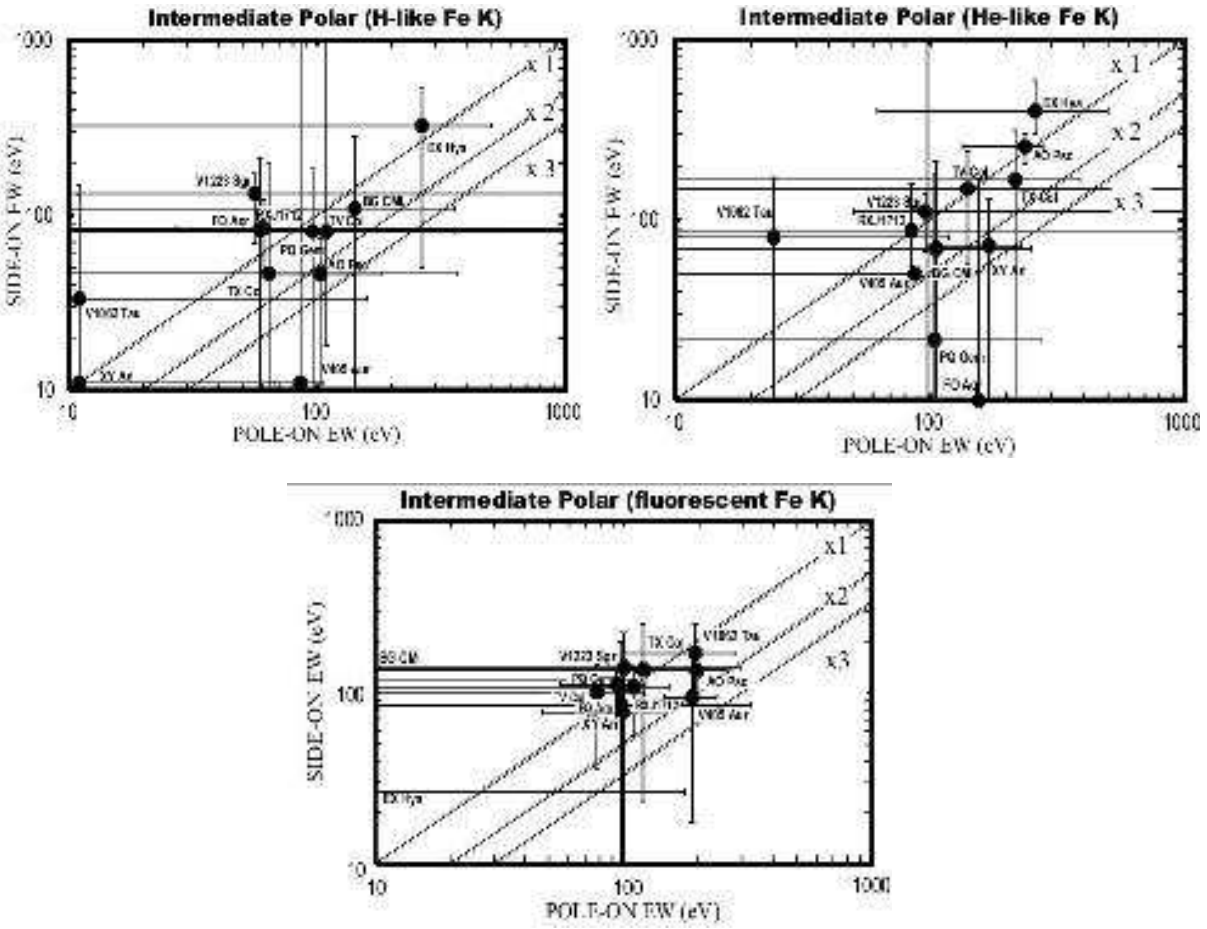


Fig. 6. The same as figure 5, but for the IPs.

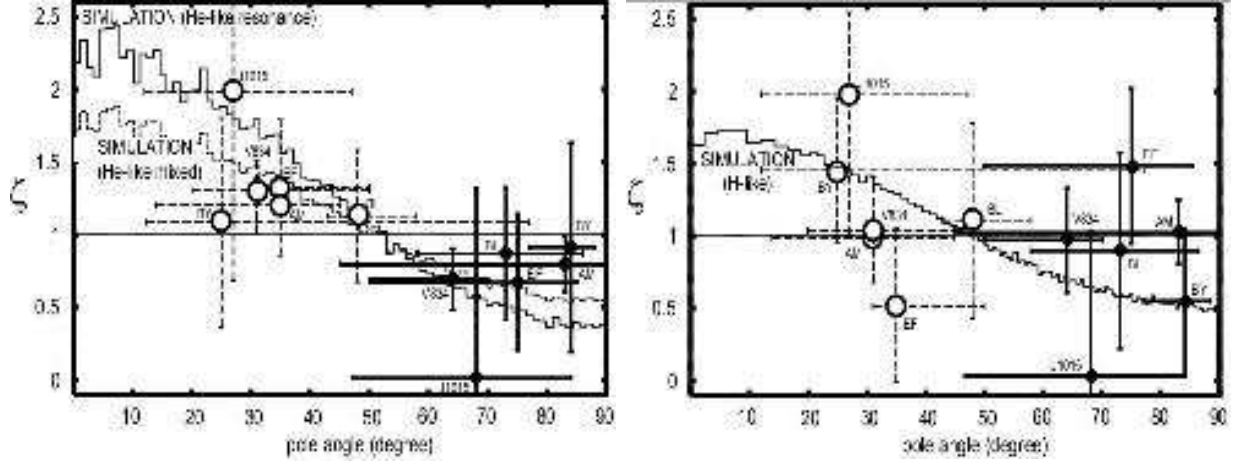


Fig. 7. The EWs of helium-like (left) and H-like (right) Fe lines of the 7 polars in their pole-on and side-on phases, relative to the phase-averaged value. The data of V2301 Oph are not plotted, because the geometrical parameters are not available. They are presented against the pole angle θ , which is calculated using the geometrical parameters in table 4 of Paper I. Each object appears twice, with the circle for pole-on data and with the filled diamond for side-on data. The angular distributions predicted by the Monte Carlo simulation (Paper I) in the nominal case are also plotted, assuming a temperature of 16 keV, the bulk velocity of the plasma of 0.9×10^8 cm s $^{-1}$, the electron density of 7.7×10^{15} cm $^{-3}$ just below the shock front, and the column radius of 7.0×10^7 cm.

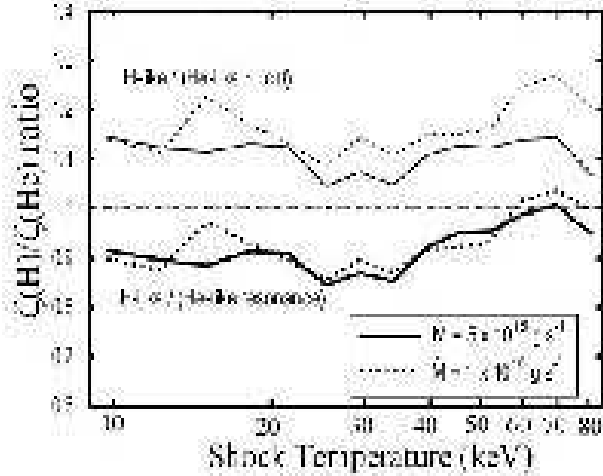


Fig. 8. Comparison of the anisotropic effects for the H-like and He-like Fe K_α lines, based on our Monte-Carlo simulation. The ratio of the enhancement ζ at the exact pole-on direction ($\theta = 0$) of H-like and He-like Fe K_α lines is shown as a function of mass-accretion rate 5×10^{16} g s $^{-1}$ and 1×10^{16} g s $^{-1}$. Calculations were done for the same sets of conditions as Paper I (shown in the caption to figure 7).

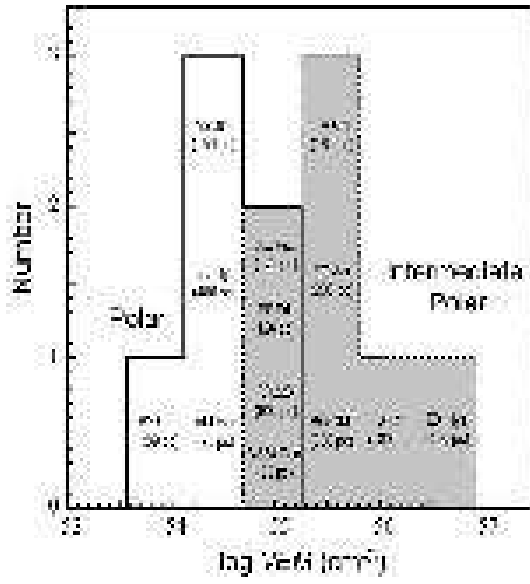


Fig. 9. The distribution of the measured emission measure of polars (thick solid histogram) and IPs (dashed lines with shadows) shown in table 1. The object names and their distances are also shown in this figure.